CoSIR: Managing an Epidemic via Optimal Adaptive Control of Transmission Policy

Harsh Maheshwari*
Flipkart Internet Private Limited
Bangalore, India
harsh.maheshwari@flipkart.com

Shreyas Shetty*
Flipkart Internet Private Limited
Bangalore, India
shreyas.shetty@flipkart.com

Nayana Bannur
Wadhwani AI
Mumbai, India
nayana.bannur@wadhwaniai.org

Srujana Merugu
Independent,
Bangalore, India
srujana@gmail.com

Abstract

Shaping an epidemic with an adaptive contact restriction policy that balances the disease and socioeconomic impact has been the holy grail during the COVID-19 pandemic. Most of the existing work on epidemiological models [40, 11, 17, 7] focuses on scenario-based forecasting via simulation but techniques for explicit control of epidemics via an analytical framework are largely missing. In this paper, we consider the problem of determining the optimal policy for transmission control assuming SIR dynamics [28], which is the most widely used epidemiological paradigm. We first demonstrate that the SIR model with infectious patients and susceptible contacts (i.e., product of transmission rate and susceptible population) interpreted as predators and prey respectively reduces to a Lotka-Volterra (LV) predator-prey model [8]. The modified SIR system (LVSIR) has a stable equilibrium point, an "energy" conservation property, and exhibits bounded cyclic behaviour similar to an LV system. This mapping permits a theoretical analysis of the control problem supporting some of the recent simulation-based studies [16, 29] that point to the benefits of periodic interventions. We use a control-Lyapunov approach to design adaptive control policies (CoSIR) to nudge the SIR model to the desired equilibrium that permits ready extensions to richer compartmental models. We also describe a practical implementation of this transmission control method by approximating the ideal control with a finite, but a time-varying set of restriction levels and provide simulation results to demonstrate its efficacy.

1 Introduction

The COVID-19 situation and its immense toll on human lives has highlighted the enormous public health challenges associated with managing a pandemic. In the absence of a vaccine, there are primarily three control levers available for public health officials, namely, (a) contact restrictions, (b) testing, tracing and isolation, and (c) provisioning for additional medical capacity. Of these, contact restrictions via lockdowns and social distancing have emerged as the most powerful policy instrument especially in low and middle income countries that cannot afford to scale up testing or medical capacity. Choosing the optimal level of restrictions, however, has been highly non-trivial not only because it involves a complex trade-off between the yet to be understood COVID-19 disease impact and other socio-economic disruptions, but also because of the rapidly evolving situation on the ground.

*Equal Contribution

Public health interventions related to the COVID-19 pandemic have largely been driven by scenario-based epidemiological forecasting studies [20, 17]. Current epidemiological models [40, 11, 7] incorporate spatio-temporal variations and predictive signals such as mobility to provide high fidelity forecasts. However, the decision making on contact restrictions is still fairly sub-optimal since it is based on the comparison of a few enumerated scenarios for a limited time horizon. Furthermore, forecasts based on a constant transmission rate (i.e., avg. #new people directly infected by an infectious person per time unit) convey the impression that the epidemic progression corresponds to a bell curve [40] regardless of empirical evidence to the contrary (see Fig 1). Flattening the curve till herd immunity is seen as the only choice. Epidemiological analysis is often centred around determining the height and timing of the caseload peak as well as the time to attain herd immunity. Though highly valuable, this scenario-based decision-making approach leans towards a limited reactive role for public health agencies.

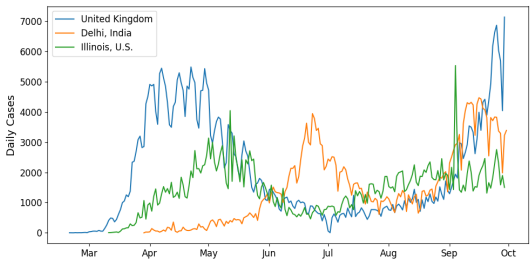

Figure 1: Daily reported infections in various regions of the world where more than one peak has been observed.

In contrast, much less attention has been devoted to developing a mathematical control framework to support proactive decision-making based on the target disease & economic outcomes, and the state of the epidemic. Multiple studies [16, 29, 13, 41] point to the benefits of periodic lockdowns and staggered mobility among population groups, but these dynamic interventions are based on forecast simulations of a limited number of scenarios and are not adaptive in nature.

In this paper, we explore the problem of optimal adaptive control of transmission rate for a desired bound on infectious population. We focus on epidemiological models based on compartmental (SIR and SEIR) dynamics [28] because of their wide applicability, parsimonious & interpretable encoding of the disease dynamics, and amenability for data-driven calibration to yield accurate forecasts.

Contributions:

- We demonstrate that the SIR dynamics map to the well-known Lotka-Volterra (LV) system [8] on interpreting infectious patients as predators and susceptible contacts (i.e., the product of transmission rate and susceptible population) as the prey under specific conditions on the transmission rate. The resulting system (LVSIR) has a well-defined stable equilibrium point and an "energy" conservation property. It exhibits a bounded cyclic trend for active infections and a steady decline of the susceptible population.
- We derive optimal control policy for transmission rate (CoSIR) using control-Lyapunov functions [45] based on the energy of the system, that is guaranteed to converge to the desired equilibrium, i.e., target infectious levels from any valid initial state. We also discuss extensions to compartmental model variants that involve an incubation period (e.g., delayed SIR, SEIR) as well as control of the infectious period that is influenced by testing and quarantine policy.
- We propose a practical approximate implementation of the transmission rate control via discrete, but time-varying restriction levels. Simulation results demonstrate the efficacy of the approximate control in stabilizing infections and adaptability to perturbations from super-spreader events [2].

The rest of the paper is organized as follows. Section 2 presents a formulation of the restriction control problem. Section 3 provides background on compartmental models, LV systems and relevant

[2] https://github.com/dsindiavscovid/sir-control

Restriction level	Effective R value	COVID-19 Transmission rate (β)	Description
Early event (Pre-restrictions)	2.52	0.4	No policy interventions.
Lockdown	0.84	0.12	Residents are either not allowed to leave their residence or may leave only for essential functions.
Stay-at-home	0.95	0.14	Stay-at-home order includes closure of schools and private sector, and restrictions on mass gatherings.
Safer-at-home	1.26	0.19	Relaxed stay-at-home order which includes closure of schools, but restrictions on mass gatherings and private sector may be relaxed.
New normal	1.83	0.29	Stay-at-home lifted or relaxed with some restrictions on mass gatherings and private sector. Schools may or may not be re-opened. Safeguards such as face coverings encouraged.

Table 1: Example of restriction levels recommended by public health authorities [1] and the corresponding effective R value and transmission rate (β) for COVID-19.

aspects of control theory. Sections 4, 5, 6, 7 present the SIR to LV system mapping, the transmission rate control mechanism, practical restriction control policy, and extensions respectively. Section 8 presents the concluding remarks.

Notation: x_t and $x(t)$ interchangeably denote the value of a variable x at time t. Time derivative of x is denoted by $\dot{x} = \frac{dx}{dt}$. $[x_t],\ [t]_{t_1}^{t_2}$ denotes the series of x as t varies from t_1 to t_2.

2 Problem Formulation

During an epidemic, a key concern for public health officials is to determine the right level and schedule of contact restrictions that balances the disease and socioeconomic burdens. Strict lockdown conditions for a short time period suppress the infection levels, but infections tend to flare up again on easing restrictions unless the epidemic is completely wiped out. On the other hand, prolonged restrictions with no intermittent easing hinder economic activity and impose heavy costs on vulnerable population groups. Furthermore, progressive reduction in the susceptible population offers a chance for relaxation of restrictions that needs to be exploited.

Modelling the multi-faceted impact of contact restrictions requires accounting for region-specific cultural and economic constructs as well as the available medical capacity, a highly complex task. For tractability, we assume that the public health goal is to limit active infections to a certain target level determined via an independent impact analysis [2]. The controls available to the public health authorities can be viewed as multiple knobs that can be set to different levels (e.g., public transport at 50% occupancy). However, the need to communicate the policy to the general public and ensure compliance entails a simpler strategy centred around a few discrete restriction levels [4, 1], (e.g. Table 1) and a preset schedule for a future time horizon, which is often longer than the intervals at which the epidemic observations are collected. For example, the infection levels might be monitored at a daily frequency, but the restriction guidelines (e.g., Level 2 on weekdays and Level 1 on weekends) might be chosen for a monthly period.

Restriction Control. For a given region, let N, S_{curr}, I_{curr} be the total, current susceptible, and infectious populations respectively. Let I_{avg}^{target} be the target average infectious level. Let $\mathcal{A}$ be the set of restriction levels for which the transmission rate is known or can be estimated[3] and T, the

[3]Mapping restriction policies to transmission rates is itself the focus of multiple studies [31, 18] but not the primary concern in the current work.

decision horizon duration, then the goal is to identify restriction levels $[a_t],\ [t]_{curr}^{curr+T},\ a_t \in \mathcal{A}\ s.t.$ the infectious level averages around I_{avg}^{target}.

Example. On Oct 1, 2020, a hypothetical city has a population of 13M of which 0.2M are currently infectious and 0.2M are post-infectious with the rest still susceptible. Assuming five restriction levels with transmission rates of $[0.1, 0.2, 0.3, 0.4, 0.5]$, the objective is to figure out a restriction policy for the upcoming month so that the infectious count averages around $I_{avg}^{target} = 150,000$.

Since our primary focus is on an analytical control framework, we make simplifying assumptions on the observability, (i.e., accurate estimates of the infectious population is possible via a mix of sero-surveys and diagnosis tests) and the infection dynamics (region isolation, homogeneous interactions, negligible incubation period, and constant infectious period). Section 7 describes extensions when some of these assumptions are relaxed.

3 Background and Related Work

Our work builds on three research areas: (a) compartmental epidemiological models, (b) Lotka-Volterra systems, and (c) optimal control of non-linear dynamical systems.

3.1 Compartmental Models

Infectious diseases are commonly modeled using compartmental models where the population (N) is divided into various compartments corresponding to different disease stages and the inter-compartment transitions are governed by the model dynamics.

The SIR model [28, 21] is the simplest and most widely used one. The model comprises three compartments: Susceptible (**S**), Infectious (**I**) and Removed (**R** - includes immune & post-infectious persons) with the dynamics in Fig 2(b). Here β is the rate of disease transmission from infectious to susceptible individuals, which largely depends on the contact restriction policy. γ is the inverse of the average infectious period, which depends on the testing and quarantine policy but is largely invariant when testing volumes are low [10]. In this model, the effective reproduction number (avg. #direct infections from each infection) is $R_{eff} = \frac{\beta S}{\gamma N}$. Existing restriction control approaches [44] are often guided by the principle of ensuring $R_{eff} \simeq 1$.

Certain infectious diseases have a significant incubation period when the individuals are infected but are not spreading the disease (non-infectious). The SEIR model [23] includes an additional **E** (exposed) compartment to model the incubation phase.

3.2 Lotka-Volterra Systems

Lotka-Volterra (LV) systems [8, 48, 25] model the population dynamics of predator-prey interactions in a biological ecosystem. These models form a special case of Kolmogorov systems [22] that capture the evolution of a stochastic process over time. In a simple 2-species LV system, the population of prey (p) interacts with that of predator (q). The growth rate of prey depends on its reproduction rate (r) and the rate of consumption by predator (e). The change in predator population depends on the nourishment-based birth rate b and its death rate d. The system has two fixed points: (a) a saddle point that maps to extinction $(p, q) = (0, 0)$, and (b) a stable equilibrium at $(p, q) = (\frac{d}{b}, \frac{r}{e})$. Typically, the system exhibits oscillations resulting in a closed phase plot that corresponds to conservation of an "energy" function. Fig 2(a) presents the dynamics of an LV system and the oscillations of the prey and predator populations. Due to the criticality of ecological population control, there has been considerable research on multiple variants of LV systems [22, 47] and their Hamiltonian dynamics [35].

3.3 Optimal Control Strategies

Optimal control of dynamical systems has rich connections to multiple fields [38] that deal with optimizing sequential decisions to maximize a desired objective such as reinforcement learning [15], multi-armed bandits [12], and stochastic control. Given a set of control variables, the optimal control policy describes the time derivatives of these variables that minimize the cost function and can be derived using Pontryagin's maximum principle [38] or the Hamilton-Jacobi-Bellman equations [37].

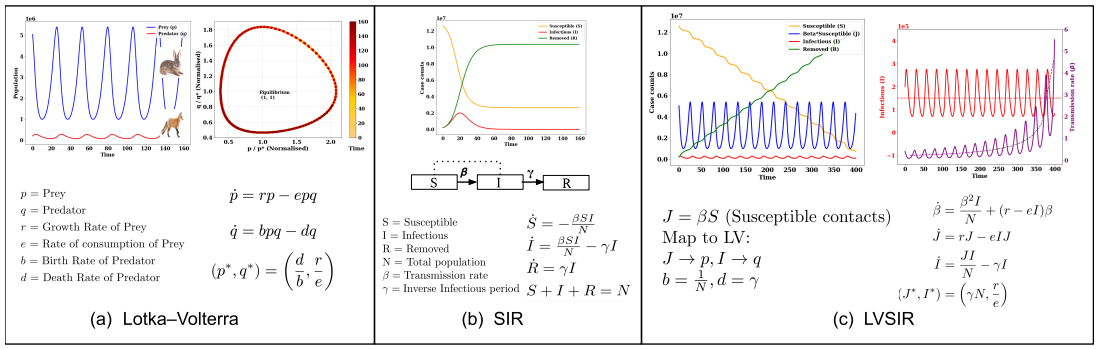

Figure 2: (a) Lotka-Volterra system and evolution of predator (fox) and prey (hare) population over time, (b) SIR compartmental dynamics for epidemiological modeling, (c) Mapping of SIR model to LV system and the temporal behaviour of case counts S, J, I, R and transmission rate β.

Though there exist comprehensive techniques for control of linear dynamical systems, the control strategies for non-linear dynamical systems rely heavily on the existence of control-Lyapunov functions, which are typically identified using conservation laws of the associated physical systems. Once a suitable Lyapunov function is identified, there exist multiple control design strategies such as feedback linearization, backstepping and sliding mode control that are guaranteed to converge using Artstein's theorem [43]. In the case of the SIR model, a suitable Lyapunov function is not readily evident. On the other hand, Lyapunov stability and practical control strategies of LV systems have been extensively studied [34, 36, 32, 19].

4 Mapping SIR to Lotka-Volterra System (LVSIR)

Our primary goal is to solve the contact restriction control problem in Section 2. We choose to mainly focus on SIR dynamics because it captures the core disease spread mechanism that is an essential element of most epidemiological models. Since existing work on stability analysis of SIR models [5] does not address controllability, we first establish a connection between the SIR model and LV system, which is more amenable to principled control. In Section 5, we leverage the properties of the LV system to propose strategies for restriction control.

The problem of stabilizing infection levels assuming SIR dynamics has a direct analogy with population control in LV predator-prey systems where it is desirable to maintain the predator and prey population at certain target levels suitable for the ecosystem. Comparing the SIR and LV dynamics in Fig 2, we observe that the behaviour of the infectious people (I) is similar to that of the "predators" (q). There is an inflow (birth) $\beta SI/N$ that depends on β as well as the current infectious & susceptible population and an outflow (death) γI from the **I** to the **R** compartment. However, the counterpart for the "prey" is not readily apparent.

An intuitive choice for "prey" is the "susceptible contacts" (i.e., the product of susceptible people and β, the #contacts of an infectious person per day) since this acts as "nourishment" to the predators and contributes to the inflow into the **I** compartment. Denoting the susceptible contacts by $J = \beta S$, we note that equivalence with the LV system requires

$$\dot{J} = \dot{\beta} S + \dot{S}\beta = (r - eI)J = (r - eI)\beta S. \tag{1}$$

Hence, the transmission rate β has to follow

$$\dot{\beta} = (r - eI)\beta - \frac{\beta^2 I}{N}. \tag{2}$$

This modified version of SIR model (LVSIR) maps to a Lotka-Volterra system. Comparing the model parameters, we note that the inverse of the infectious period (γ) corresponds to the predator death rate (d) and the inverse of population ($1/N$) to the predator birth rate (b). We now analyze the behaviour of the LVSIR system.

Theorem 1 [4] *For the LVSIR model in Fig. 2(c), the following holds true:*

[4] Please see Appendix A for the proofs.

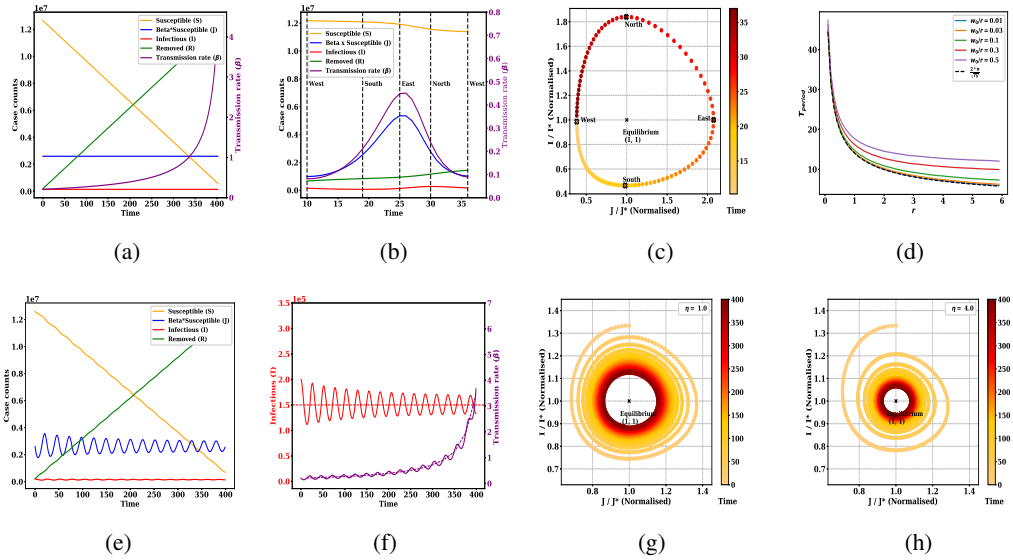

Figure 3: Plots (a-d) and (e-h) present the dynamics of LVSIR and CoSIR models respectively. (a) System (S, J, I, R, β) evolution when initialized at equilibrium, (b-c) Single period of oscillations and normalized phase plot for the configuration in Fig 2(c) annotated with the extreme points, (d) Dependence of T_{period} on r for different choices of w_0/r. (e-f) System evolution of the CoSIR model for learning rate $\eta = 1$. (g-h) Normalized phase plots of CoSIR model for $\eta = 1$ and 4.

1. *There exists a stable equilibrium at* $(J^*, I^*) = (\gamma N, r/e)$.
2. *When the initial state* $(J_0, I_0) = (J^*, I^*)$, *then* (J, I) *remain constant while* S, R *take a linear form and* β *increases till the susceptible population reaches 0 at* T_{end}.
   (i) $S(t) = S_0 - \gamma I^* t; \;\; R(t) = R_0 + \gamma I^* t$
   (ii) $\beta(t) = \frac{\gamma N}{S_0 - \gamma I^* t}; \;\; T_{end} = \frac{S_0}{\gamma I^*}$

Theorem 2 *For the LVSIR model in Fig. 2(c), if the initial state is not at equilibrium, i.e.,* $(J_0, I_0) \neq (J^*, I^*)$, *it exhibits a cyclic behaviour with the following properties.*

1. *The system "energy"* $w(J, I) = \gamma(x - \log(x) - 1) + r(y - \log(y) - 1)$ *(where* $x = \frac{J}{J^*}, y = \frac{I}{I^*}$*) remains constant at* $w_0 = w(J_0, I_0) \geq w(J^*, I^*) = w^* = 0$ *till termination.*
2. *The* I, J *curves exhibit periodic oscillations resulting in a closed trajectory. The normalized phase plot has four extreme points* $\{(x_{min}, 1), (1, y_{min}), (x_{max}, 1), (1, y_{max})\}$ *where* (x_{min}, x_{max}) *are the roots of the equation* $x - \log(x) = 1 + w_0/\gamma$ *and* (y_{min}, y_{max}) *are the roots of the equation* $y - \log(y) = 1 + w_0/r$.
3. *The cyclic period is given by*
   $$T_{period} = \int_{\log(x_{min})}^{\log(x_{max})} \left(\frac{1}{F_1^{-1}(G(z))} - \frac{1}{F_2^{-1}(G(z))}\right) dz,$$
   where (x_{min}, x_{max}) *are defined as above,* $G(z) = \gamma(e^z - z - 1) - w_0$, *and* $F_1(s),\ F_2(s)$ *are restrictions of* $F(s) = s + r\log(1 - \frac{s}{r})$ *to +ve and -ve ranges. In general,* T_{period} *has the form* $g(r, \gamma, \frac{w_0}{r})$ *with approximation via linearization yielding* $T_{period} \simeq \frac{2\pi}{\sqrt{(r\gamma)}}$.
4. *In each cyclic period,* S *reduces by a fixed amount* $\Delta S = \gamma I^* T_{period}$. *When the susceptible population* $S < \Delta S$ *at the beginning of a cycle, it reaches* 0 *during the cycle and the epidemic terminates.*

Fig 2(c) depicts the oscillatory behaviour of the LVSIR model for the configuration in Table 2. Similar to an LV system, the "energy" which corresponds to a weighted Itakura-Saito distance [26] between

(I, J) and the equilibrium (I^*, J^*) is conserved. The infectious population I (and susceptible contacts J) oscillates between $[y_{min}I^*, y_{max}I^*]$ (and $[x_{min}J^*, x_{max}J^*]$) during the entire period with an average value of I^* (and J^*) while the susceptible population reduces steadily in a staircase-like fashion. The transmission rate β also exhibits periodic oscillations but the average steadily goes up to compensate for the reduction in the susceptible population. Fig 3(c-b) shows the phase plot and the variation of the key quantities during a single period with the four extreme points (South, East, North, West) marked explicitly. Fig 3(d) shows how T_{period} [42] depends on r for different choices of w_0/r. This mapping can be used to identify suitable values of r for practical policy making. For the special case where the initial state is at equilibrium, the system behaviour is steady as in Fig 3(a).

5 CoSIR: Transmission Control

We now consider the problem of controlling the transmission rate β for the LVSIR model (Fig 2(c)) to nudge the infectious levels to a desired equilibrium. As discussed in Section 3, control of non-linear dynamical systems is typically achieved via Control-Lyapunov functions (CLFs). Our approach is to exploit the mapping from the SIR model to LV system and use CLFs derived from the "Lotka-Volterra energy" function $w(J, I)$.

Given a dynamical system $\dot{\mathbf{z}} = \mathbf{f}(\mathbf{z}, \mathbf{u})$ with state vector $\mathbf{z} \in D \subset \mathbb{R}^n$, control $\mathbf{u} \in \mathbb{R}^m$, and equilibrium state $\mathbf{z}^* = \mathbf{0}$, a control-Lyapunov function (CLF) is a function $V : D \mapsto \mathbb{R}$ that is continuously differentiable, positive-definite s.t. $\forall \mathbf{z} \neq 0, \exists\, \mathbf{u}, \dot{V}(\mathbf{z}, \mathbf{u}) = \langle \nabla V(\mathbf{z}), \dot{\mathbf{z}} \rangle = \langle \nabla V(\mathbf{z}), \mathbf{f}(\mathbf{z}, \mathbf{u}) \rangle < 0$.

The CLF $V(\cdot)$ can be viewed as a generalized energy function with $\dot{V}(\cdot)$ being a dissipation function. Artstein [6] proved that as long as there is a CLF, there exists a control $\mathbf{u}$ to ensure the reduction of energy at every non-equilibrium state and eventual convergence to the zero energy equilibrium.

Theorem 3 (Artstein) *For any non-linear dynamical system with affine control, $\dot{\mathbf{z}} = \mathbf{f}(\mathbf{z}, \mathbf{u}) = \mathbf{f_0}(\mathbf{z}) + \sum_{i=1}^{m} \mathbf{f_i}(\mathbf{z}) u_i$ with state $\mathbf{z} \in D \subset \mathbb{R}^n$, control $\mathbf{u} \in \mathbb{R}^m$, has a CLF if and only if it admits a regular stabilizing control feedback $\mathbf{u}$, that is a locally Lipschitz function on $\mathbb{R}^n \setminus \{0\}$.*

Once a CLF is identified, it is relatively straightforward to design an appropriate control function $\mathbf{u}$ as described in [6, 46]. For our scenario, we rely on the conservation law of the LV system as well as the existing literature on its Lyapunov functions [39].

Let $\mathbf{z} = (\frac{J}{J^*} - 1, \frac{I}{I^*} - 1)$ so that the equilibrium $\mathbf{z}^* = (0, 0)$. Let $L(a_1, a_2) : \mathbb{R}_+^2 \mapsto \mathbb{R}$ be a continuously differentiable divergence such that $|\frac{dL}{da_1}| > 0$ and $L(a_1, a_2) > 0,\ \forall a_1 \neq a_2$ and $L(a_1, a_2) = 0 \iff a_1 = a_2$. Then, the function $V(\mathbf{z}) = L(w, w^{target})$ where $w = w(J, I)$ can be used as a CLF. We focus on the case where $w^{target} = w^* = 0$. and propose a controlled SIR model (CoSIR).

Theorem 4 (CoSIR) *For the SIR model, a proportional additive control on β,*

$$\dot{\beta} = \frac{\beta^2 SI}{N} + (r - eI)\beta + u\beta \tag{3}$$

converges to the equilibrium (J^*, I^*) when

$$u = -\eta(t) \frac{dL}{dw} \left(\frac{J}{J^*} - 1 \right)$$

and the learning rate $\eta(t) > 0,\ \forall t$.

A special case of the above construction with $V(\mathbf{z}) = L(w, w^*) = \frac{1}{2}(w - w^*)^2$ and a constant positive learning rate η referred to as the speed-gradient method was proposed by [36] in the context of population control. The resulting control policy is given by

$$u = -\eta(w(J, I) - w^*) \left(\frac{J}{J^*} - 1 \right). \tag{4}$$

Fig 3(e-f) show the behavior of the CoSIR model using Eqn. 4 and parameters from Table 2. It can be observed that the oscillations reduce with time and the I, J curves converge to the equilibrium with

Static parameters	Population	N	13 M
Initial state	Stage of epidemic	(S_0, I_0, R_0)	(12.6M, 0.2M, 0.2M)
Public health requirements	Target infectious level	I_{avg}^{target}	0.15M
	Restriction periodicity	T_{period}	7 days
SIR parameters	Reciprocal of infectious period	γ	0.2
CoSIR parameters	Initial transmission rate	$\beta_0 = \frac{\gamma N}{S_0}$	0.206
	Reproductive & consumption rates	(r, e)	(4.2, 2.8×10^{-5})
	Learning rate	η	5

Table 2: Epidemic state, public health requirements, and CoSIR model parameters corresponding to the scenario in Section 2.

the convergence rate dependent on η. The design of the control also makes it robust to perturbations in the infectious population as the system re-calibrates β as appropriate.

The β-control policy (Eqn. 3) can be interpreted as follows. The first term $\frac{\beta^2 I}{N}$ corresponds to the relaxation possible due to the decreasing susceptible population while the second term $(r - eI)\beta$ leads to oscillatory behavior, and the last term $u\beta = -\eta(t)\beta\frac{dL}{dw}(J/J^* - 1)$ ensures dissipation of energy and convergence to the equilibrium.

6 Practical Transmission Control

We now describe a practical solution to the public health restriction control problem in Section 2. Algorithm 1 outlines a holistic approach to obtain a restriction schedule using the optimal β-control in Theorem 4. There are four key steps.

Input Collection. Infection level targets (I_{avg}^{target}, I_{max}^{target}), periodicity of the restriction schedule (T_{period}), decision horizon (T) need to be determined based on a careful assessment of public health and socioeconomic considerations. Historical case counts and restrictions ($[S_t, I_t, R_t, a_t],\ [t]_0^{curr}$) also need to be collected to enable accurate optimization.

Data-driven Calibration. The next step is to use SIR-calibration methods [40, 11, 7] along with historical data to estimate a static γ, time-varying β, and the state of the epidemic ($S_{curr}, I_{curr}, R_{curr}$). The restriction level to transmission map, π, can be initially chosen from public health guidelines [1] and refined using the observed β for past restrictions in the region of interest.

Choosing CoSIR Parameters. The free parameters of the CoSIR model need to be chosen based on the control requirements. Algorithm 1 lists the updates derived from Theorem 2 with flexibility on the choice of $\hat{\beta}_{curr}$ and η. Choosing the immediate transmission rate to be $\hat{\beta}_{curr} = \frac{J^*}{S_{curr}} = \frac{\gamma N}{S_{curr}}$ (equivalent to forcing effective reproduction number $R_{eff} = 1$) ensures a maximal reduction in the system "energy" and faster convergence to the desired equilibrium, but dampens fluctuations. However, fluctuations might be necessary for economic activity. When nearly steady infection levels are desired, $I_{avg}^{target} \simeq I_{max}^{target}$, then $r = \frac{(2\pi)^2}{\gamma T_{period}^2}$ and high η are appropriate.

Computing Optimal Restrictions. Determining the optimal policy can be split into two phases. The first involves estimating the ideal β control from Eqn. 4 while the second involves identifying the "closest" restriction level for the ideal β at each time step with "closeness" based on a suitable divergence such as the squared loss.

Employing Algorithm 1 for the scenario in Example 1 with a weekly periodicity, we obtain suitable parameters (Table 2) for the CoSIR model. Fig 4 shows the behaviour with three variants of restriction policies (`arbitrary`, CoSIR, and CoSIR-APPROXIMATION based on the specified levels). In case of the arbitrary policy, the infections peak in narrow time intervals and become unmanageable while the ideal CoSIR and even approximate control variants are able to achieve a steady rate of infections. This is true even when the infection levels are subject to sudden upward ($t = 50$) or downward perturbations ($t = 100$) in case of super-spreader events or sudden quarantine restrictions respectively. The β-control mechanism adapts and continues to push towards the equilibrium.

Algorithm 1 CoSIR: Transmission Control

Input:
N – Population,
$\mathcal{A}$ – Restriction policy levels,
$\pi : \mathcal{A} \mapsto \mathbb{R}_{++}$ – Map of levels to transmission rate,
$[S_t, I_t, R_t, a_t], [t]_0^{curr}$ – Case counts & restriction history,
$I_{max}^{target}, I_{avg}^{target}$ – Max and avg., target infection levels,
T – Decision horizon,
T_{period} – Cyclic period for restriction schedule
Output:
$\mathbf{a}^* = [a_t],\ [t]_{curr}^{curr+T},\ a_t \in \mathcal{A}$ – Near optimal restriction levels for next T time units s.t. infection levels conform to $I_{max}^{target}, I_{avg}^{target}$.
Method:
Data-driven Calibration:
$\gamma \leftarrow \textsc{ComputeGamma}([S_t, I_t, R_t],\ [t]_0^{curr}, N)$
$\pi \leftarrow \textsc{RefineBetaMap}(\pi, [S_t, I_t, R_t, a_t],\ [t]_0^{curr}, N)$
Choosing CoSIR Parameters:
$\hat{\beta}_{curr} \leftarrow \frac{\gamma N}{S_{curr}}$
$(J^*, I^*) \leftarrow (\gamma N, I_{avg}^{target})$
$\alpha \leftarrow (y - \log(y) - 1)$ where $y = \frac{I_{max}^{target}}{I_{avg}^{target}}$
$r \leftarrow \frac{(2\pi)^2}{\gamma T_{period}^2}$ for $\alpha \simeq 0$
(or chosen s.t. $g(r, \gamma, \alpha) = T_{period}$ for $\alpha >> 0$).
$e \leftarrow \frac{r}{I^*}$
$\eta \leftarrow$ desired convergence rate
Determine Optimal Restrictions:
$[\beta_t^{ideal}],\ [t]_{curr}^{curr+T} \leftarrow \textsc{CoSIR}(N, S_{curr}, I_{curr}, R_{curr}, \hat{\beta}_{curr}, r, e, \gamma, \eta, T)$
$a_t = \text{argmin}_{a \in \mathcal{A}}\ (\beta_t^{ideal} - \pi(a))^2,\ [t]_{curr}^{curr+T}$
return $\mathbf{a}^* = [a_t],\ [t]_{curr}^{curr+T}$

7 Extensions

We now briefly describe some key extensions.

Delayed SIR & SEIR Models. The SEIR model allows explicit modelling of the incubation period and is known to closely mimic the behaviour of the delayed SIR model [27]. When β follows Eqn. 2, the delayed SIR model readily maps to a delayed LV system with a non-preying growth period for the predators, which is a special case of the well-studied Wangersky–Cunningham systems [33, 47]. It can be shown that the modified delayed SIR system with a delay τ has the same equilibrium $(J^*, I^*) = (\gamma N, r/e)$, exhibits (unbounded) oscillations and permits control of the form Eqn 3, where

$$u(t) = -\eta(t)\frac{dL}{dw}\left(\frac{J(t)}{J^*} - 1\right) - r\left(\frac{(I(t) - I^*)}{(J(t) - J^*)}\right)\left(\frac{J(t-\tau)I(t-\tau) - J(t)I(t)}{I(t)I^*}\right)$$

with $\eta(t) > 0$. There is a need for special handling when J approaches J^* with the behavior depending on τ.

Testing & Isolation Policy. Testing, tracing and isolation also play a critical role in regulating the epidemic. In terms of SIR and SEIR dynamics, the net effect of aggressive testing is minimizing the infectious period or increasing γ [9, 30]. This is analogous to the culling of predators (infectious population) by increasing the death rate for which there already exist multiple control mechanisms [34]. In particular, choosing $V(\mathbf{z}) = L(w(J, I), w^*)$ as the control-Lyapunov function of interest, we obtain the control, $\gamma(t) = \gamma_0 + \zeta(t)\frac{dL}{dw}(\frac{I}{I^*} - 1)$, with $\zeta(t) > 0$.

Online Learning. The restriction control problem can also be posed as a non-linear contextual bandit [12] formulation with the cumulative LV energy $w(J, I)$ of the CoSIR model over a future horizon interpreted as the (negative) "reward". Here, the discrete restriction levels can be viewed

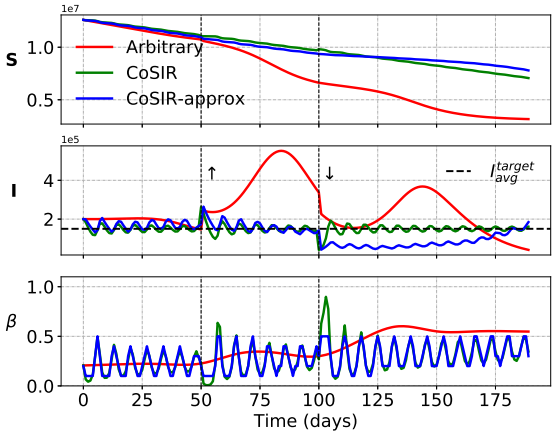

Figure 4: Disease progression (S, I, β) with three restriction policies: `arbitrary`, CoSIR and CoSIR-APPROXIMATION (using specified levels). The CoSIR variants maintain infectious counts close to target levels and also adapt to a sudden increase ($t = 50$) or decrease ($t = 100$).

as the multiple arms of a bandit, the context includes the state of the epidemic, and the "reward" distribution is computed using the context and the observed transmission rate for the arms.

8 Conclusion & Future Directions

Our current work proposes an analytical framework for epidemic control with the intent of supporting an active goal-oriented public health response. The proposed framework relies on a mapping between SIR dynamics to Lotka-Volterra systems under specific conditions on the transmission rate. Given the vast literature on control of LV systems, this mapping can be leveraged to design new epidemic control techniques as well as extend current results to richer heterogeneous compartmental models and additional control variables (e.g., testing levels). Effective practical implementation of control requires further exploration of online and reinforcement learning variants [38], addressing the limitations of SIR dynamics, and incorporation of additional signals such as mobility [3]. This effort also points to the feasibility of exploring control strategies for other macro social and physical systems, e.g., good and bad actor populations on social media.

References

[1] Analysis and mapping of policies - COVID-AMP, 2020. Accessed October 2, 2020. URL: `https://covidamp.org/`.

[2] COVID-19: A Global Perspective, 2020. URL: `https://www.gatesfoundation.org/goalkeepers/report/2020-report/#GlobalPerspective`.

[3] Google mobility data, 2020. Accessed October 2, 2020. URL: `https://www.google.com/covid19/mobility/`.

[4] New Zealand COVID-19 alert levels, 2020. Accessed October 2, 2020. URL: `https://covid19.govt.nz/assets/resources/tables/COVID-19-alert-levels-detailed.pdf`.

[5] Phillipe Adda and Derdei Bichara. Global stability for SIR and SIRS models with differential mortality. *International Journal of Pure and Applied Mathematics*, 80(3):425–433, 2012.

[6] Zvi Artstein. Stabilization with relaxed controls. *Nonlinear Analysis: Theory, Methods & Applications*, 7(11):1163–1173, 1983. `doi:10.1016/0362-546X(83)90049-4`.

[7] Jackie Baek, Vivek F. Farias, Andreea Georgescu, Retsef Levi, Tianyi Peng, Deeksha Sinha, Joshua Wilde, and Andrew Zheng. The limits to learning an SIR process: Granular forecasting for COVID-19, 2020. arXiv:2006.06373.

[8] Stephen Baigent. Lotka-Volterra dynamics: An introduction. 2016. URL: https://www.ucl.ac.uk/~ucess29/LTCC_LV2010.pdf.

[9] Yinon M. Bar-On, Ron Sender, Avi I. Flamholz, Rob Phillips, and Ron Milo. A quantitative compendium of COVID-19 epidemiology, 2020. arXiv:2006.01283.

[10] David W Berger, Kyle F Herkenhoff, and Simon Mongey. An SEIR infectious disease model with testing and conditional quarantine. Technical report, National Bureau of Economic Research, 2020. URL: https://www.nber.org/papers/w26901.

[11] Luís M. A. Bettencourt and Ruy M. Ribeiro. Real time Bayesian estimation of the epidemic potential of emerging infectious diseases. *PLOS ONE*, 3(5):1–9, 2008. URL: https://journals.plos.org/plosone/article?id=10.1371/journal.pone.0002185.

[12] Alina Beygelzimer, John Langford, Lihong Li, Lev Reyzin, and Robert Schapire. Contextual bandit algorithms with supervised learning guarantees. In *Proceedings of the Fourteenth International Conference on Artificial Intelligence and Statistics*, pages 19–26, 2011. URL: http://proceedings.mlr.press/v15/beygelzimer11a.html.

[13] Michelangelo Bin, Peter Cheung, Emanuele Crisostomi, Pietro Ferraro, H. Lhachemi, R. Murray-Smith, Connor Myant, Thomas Parisini, Robert Shorten, S. Stein, and L. Stone. On fast multi-shot COVID-19 interventions for post lock-down mitigation, 2020. arXiv:2003.09930.

[14] W.E. Boyce, R.C. DiPrima, and D.B. Meade. *Elementary Differential Equations and Boundary Value Problems*. Wiley, 2017. URL: https://books.google.co.in/books?id=SyaVDwAAQBAJ.

[15] Yinlam Chow, Ofir Nachum, Edgar Duenez-Guzman, and Mohammad Ghavamzadeh. A Lyapunov-based approach to safe reinforcement learning. In *Advances in Neural Information Processing Systems*, pages 8092–8101, 2018.

[16] Rajiv Chowdhury, Kevin Heng, Md Shajedur Rahman Shawon, Gabriel Goh, Daisy Okonofua, Carolina Ochoa-Rosales, Valentina Gonzalez-Jaramillo, Abbas Bhuiya, Daniel Reidpath, Shamini Prathapan, et al. Dynamic interventions to control COVID-19 pandemic: a multivariate prediction modelling study comparing 16 worldwide countries. *European Journal of Epidemiology*, 35(5):389–399, 2020. doi:10.1007/s10654-020-00649-w.

[17] IHME COVID, Christopher JL Murray, et al. Forecasting the impact of the first wave of the COVID-19 pandemic on hospital demand and deaths for the USA and European economic area countries. *medRxiv*, 2020. doi:10.1101/2020.04.21.20074732.

[18] Amélie Desvars-Larrive, Elma Dervic, Nils Haug, Thomas Niederkrotenthaler, Jiaying Chen, Anna Di Natale, Jana Lasser, Diana S. Gliga, Alexandra Roux, Johannes Sorger, Abhijit Chakraborty, Alexandr Ten, et al. A structured open dataset of government interventions in response to COVID-19. *Scientific Data*, 7(1):285, 2020. doi:10.1038/s41597-020-00609-9.

[19] Awad El-Gohary and M.T. Yassen. Optimal control and synchronization of Lotka–Volterra model. *Chaos, Solitons & Fractals*, 12(11):2087 – 2093, 2001. doi:10.1016/S0960-0779(00)00023-0.

[20] Neil Ferguson, Daniel Laydon, Gilani G Nedjati, N Imai, K Ainslie, M Baguelin, S Bhatia, A Boonyasiri, Perez Z Cucunuba, G Cuomo-Dannenburg, A Dighe, et al. Report 9: Impact of non-pharmaceutical interventions (NPIs) to reduce COVID19 mortality and healthcare demand. Technical report, Imperial College, London, 2020. doi:10.25561/77482.

[21] Tiberiu Harko, Francisco S.N. Lobo, and M.K. Mak. Exact analytical solutions of the susceptible-infected-recovered (SIR) epidemic model and of the SIR model with equal death and birth rates. *Applied Mathematics and Computation*, 236:184 – 194, 2014. doi:10.1016/j.amc.2014.03.030".

[22] Alexandru Hening and Dang H. Nguyen. Coexistence and extinction for stochastic Kolmogorov systems. *Annals Applied Probability*, 28(3):1893–1942, 06 2018. doi:10.1214/17-AAP1347.

[23] Herbert W Hethcote. The mathematics of infectious diseases. *SIAM review*, 42(4):599–653, 2000. doi:10.1137/S0036144500371907.

[24] Sze-Bi Hsu. A remark on the period of the periodic solution in the Lotka-Volterra system. *Journal of Mathematical Analysis and Applications*, 95(2):428–436, 1983. doi:10.1016/0022-247X(83)90117-8.

[25] Timon Idema. The behaviour and attractiveness of the Lotka-Volterra equations. Master's thesis, Universiteit Leiden, 2005. URL: https://www.sas.upenn.edu/~tidema/publications/maththesis.pdf.

[26] Fumitada Itakura and Shuzo Saito. Analysis synthesis telephony based upon the maximum likelihood method. pages 17–20, 1968.

[27] Abdelilah Kaddar, Abdelhadi Abta, and Talibi Hamad. A comparison of delayed SIR and SEIR epidemic models. *Nonlinear Analysis. Modelling and Control*, 2:181–190, 2011. doi:10.15388/NA.16.2.14104.

[28] William Ogilvy Kermack and Anderson G McKendrick. A contribution to the mathematical theory of epidemics. *Proceedings of the Royal Society of London*, 115(772):700–721, 1927. doi:10.1098/rspa.1927.0118.

[29] Jackson A. Killian, Marie Charpignon, Bryan Wilder, Andrew Perrault, Milind Tambe, and Maimuna S. Majumder. Evaluating COVID-19 lockdown and business-sector-specific reopening policies for three US states. In *KDD 2020 Workshop on Humanitarian Mapping*, 2020. doi:10.2139/ssrn.3598744.

[30] Daniel B Larremore, Bryan Wilder, Evan Lester, Soraya Shehata, James M Burke, James A Hay, Milind Tambe, Michael J Mina, and Roy Parker. Test sensitivity is secondary to frequency and turnaround time for COVID-19 surveillance. *MedRxiv*, 2020. doi:10.1101/2020.06.22.20136309.

[31] Lukas Lehner. COVID19 policy trackers, 2020. URL: https://lukaslehner.github.io/covid19policytrackers/.

[32] A. Magyar, G. Szederkényi, and K.M. Hangos. Globally stabilizing feedback control of process systems in generalized Lotka–Volterra form. *Journal of Process Control*, 18(1):80 – 91, 2008. doi:10.1016/j.jprocont.2007.05.003.

[33] Annik Martin and Shigui Ruan. Predator-prey models with delay and prey harvesting. *Journal of Mathematical Biology*, 43:247–267, 2001. doi:10.1007/s002850100095.

[34] Magno Enrique Mendoza Meza, Amit Bhaya, and Eugenius Kaszkurewicz. Controller design techniques for the Lotka-Volterra nonlinear system. *SBA: Controle & Automaccão Sociedade Brasileira de Automatica*, 16:124 – 135, 2005. doi:10.1590/S0103-17592005000200002.

[35] Yavuz Nutku. Hamiltonian structure of the Lotka-Volterra equations. *Physics Letters A*, 145(1):27 – 28, 1990. doi:10.1016/0375-9601(90)90270-X.

[36] Irina Pchelkina and Alexander L. Fradkov. Control of oscillatory behavior of multispecies populations. *Ecological Modelling - ECOL MODEL*, 227:1–6, 2012. doi:10.1016/j.ecolmodel.2011.10.022.

[37] Shige Peng. Stochastic Hamilton–Jacobi–Bellman equations. *SIAM Journal on Control and Optimization*, 30(2):284–304, 1992. doi:10.1137/0330018.

[38] Warren B Powell. From reinforcement learning to optimal control: A unified framework for sequential decisions, 2019. arXiv:1912.03513.

[39] Yuri Aleksandrovich Pykh. Lyapunov functions for Lotka-Volterra systems: An overview and problems. *IFAC Proceedings Volumes*, 34(6):1549 – 1554, 2001. doi:10.1016/S1474-6670(17)35410-1.

[40] Evan L Ray, Nutcha Wattanachit, Jarad Niemi, Abdul Hannan Kanji, Katie House, Estee Y Cramer, Johannes Bracher, Andrew Zheng, Teresa K Yamana, Xinyue Xiong, Spencer Woody, Yuanjia Wang, et al. Ensemble forecasts of Coronavirus disease 2019 (COVID-19) in the U.S. *medRxiv*, 2020. doi:10.1101/2020.08.19.20177493.

[41] Snehal Shekatkar, Bhalchandra Pujari, Mihir Arjunwadkar, Dhiraj Kumar Hazra, Pinaki Chaudhuri, Sitabhra Sinha, Gautam Menon, Anupama Sharma, and Vishwesha Guttal. INDSCI-SIM A state-level epidemiological model for India, 2020. Ongoing Study at https://indscicov.in/indscisim.

[42] Shagi-Di Shih. The period of a Lotka-Volterra system. *Taiwanese Journal of Mathematics*, 1(4):451–470, 1997.

[43] Eduardo D. Sontag. A 'universal' construction of Artstein's theorem on nonlinear stabilization. *Systems & Control Letters*, 13(2):117 – 123, 1989. doi:10.1016/0167-6911(89)90028-5.

[44] Kevin Systrom, Thomas Vladek, and Mike Krieger. Rt. live. https://github.com/rtcovidlive/covid-model, 2020.

[45] John Tsinias. Stabilization of affine in control nonlinear systems. *Nonlinear Analysis: Theory, Methods & Applications*, 12(11):1283 – 1296, 1988. doi:10.1016/0362-546X(88)90060-0.

[46] John Tsinias. Sufficient Lyapunov-like conditions for stabilization. *Mathematics of Control, Signals and Systems*, 2(4):343–357, 1989. doi:10.1007/BF02551276.

[47] Peter J Wangersky and WJ Cunningham. Time lag in prey-predator population models. *Ecology*, 38(1):136–139, 1957. doi:10.2307/1932137.

[48] Xiang-Ping Yan and Yan-Dong Chu. Stability and bifurcation analysis for a delayed Lotka–Volterra predator–prey system. *Journal of Computational and Applied Mathematics*, 196(1):198 – 210, 2006. doi:10.1016/j.cam.2005.09.001.

A Proofs

Definition 1 *[14] Let $\mathbf{z}^* \in \mathbb{R}^n$ be a critical point of a system of ODEs. The critical point $\mathbf{z}^*$ is stable if, for any $\epsilon > 0$ $\exists$ $\delta > 0$ such that if $\mathbf{z} = \phi(t)$ satisfies $||\phi(0) - \mathbf{z}^*|| < \delta$ then $||\phi(t) - \mathbf{z}^*|| < \epsilon$, $\forall\, t > 0$.*

Proof of Theorem 1(a).
At equilibrium (J^*, I^*), we have $\dot{J} = 0$ and $\dot{I} = 0$. From Eqn. 1, it follows that

$$\dot{J}|_{(J,I)=(J^*,I^*)} = rJ^* - eI^*J^* = 0 \Rightarrow I^* = \frac{r}{e},$$

$$\dot{I}|_{(J,I)=(J^*,I^*)} = \frac{J^*I^*}{N} - \gamma I^* = 0 \Rightarrow J^* = \gamma N.$$

To prove the stability of the critical point at (J^*, I^*), let us consider the normalized variables $\phi(t) = \big(x(t), y(t)\big)$ where $x(t) = \frac{J(t)}{J^*}$ and $y(t) = \frac{I(t)}{I^*}$. $\mathbf{z}^* = (1, 1)$ is the corresponding critical point.

$$\begin{aligned} ||\phi(0) - \mathbf{z}^*||^2 &= (x_0 - 1)^2 + (y_0 - 1)^2 < \delta^2 \\ &\Rightarrow 1 - \delta < x_0 < 1 + \delta,\ 1 - \delta < y_0 < 1 + \delta. \end{aligned}$$

Let $f(s) = s - \log(s) - 1$. Since $f(s)$ is a convex function, $1 - \delta < s < 1 + \delta$, implies $f(s) < \max\{f(1 + \delta), f(1 - \delta)\}$. Denoting this bound by D_{max} implies $f(x_0) < D_{max}$ and $f(y_0) < D_{max}$
From Theorem 2(a), we note that

$$\begin{aligned} w(J_0, I_0) &= \gamma f(x_0) + rf(y_0) \\ &< (r + \gamma)D_{max} \end{aligned}$$

Denoting $w_b = (r+\gamma)D_{max}$, from Theorem 2(a), we note that

$$\begin{aligned} &w(J(t), I(t)) = w(J_0, I_0) < w_b \\ &\Rightarrow f\big(x(t)\big) < \frac{w_b}{\gamma}, \;\; f\big(y(t)\big) < \frac{w_b}{r}. \end{aligned}$$

Given the nature of $f(s)$, $f(s) < c \Rightarrow s_{min} < s < s_{max}$ where (s_{min}, s_{max}) are the finite-valued roots of $f(s) = c$. Hence $x(t)$ and $y(t)$ are both bounded on either side. Consequently, $(x(t)-1, y(t)-1)$ is confined to a bounded rectangle and thus,

$$\begin{aligned} \Rightarrow ||\phi\big(x(t), y(t)\big) - \mathbf{z}^*||^2 &= \big(x(t)-1\big)^2 \\ &\quad + \big(y(t)-1\big)^2 \\ &< \epsilon^2 \end{aligned}$$

where ϵ can be directly expressed in terms of δ and vice versa.
Hence, from Definition 1, $\mathbf{z}^* = (1,1)$ (or equivalently (J^*, I^*)) is a stable equilibrium. ■

Proof of Theorem 1(b).

When initial state (J_0, I_0) is at equilibrium $(J^*, I^*) = (\gamma N, r/e)$, we have $(J(t), I(t)) = (\gamma N, r/e)$, $\forall t$. Hence,

$$\dot{S} = -\frac{\beta S I^*}{N} = -\frac{J^* I^*}{N} = -\gamma I^*$$

$$\Rightarrow S(t) = S_0 - \gamma I^* t.$$

Similarly,

$$\dot{R} = \gamma I^* \Rightarrow R(t) = R_0 + \gamma I^* t,$$

$$\beta(t) = \frac{J(t)}{S(t)} = \frac{\gamma N}{S_0 - \gamma I^* t}.$$

At $t = T_{end}$, the susceptible population $S(t) = 0$. Hence,

$$S(T_{end}) = 0 \Rightarrow T_{end} = \frac{S_0}{\gamma I^*}.$$

■

Proof of Theorem 2(a).
The energy function of the LVSIR system in Fig 2(c) corresponds to

$$w(J, I) = \gamma\left(\frac{J}{J^*} - \log\left(\frac{J}{J^*}\right) - 1\right) + r\left(\frac{I}{I^*} - \log\left(\frac{I}{I^*}\right) - 1\right),$$

and the dynamics of I, J are given by

$$\dot{J} = (r - eI)J = r\left(1 - \frac{I}{I^*}\right)J$$

$$\dot{I} = \left(\frac{J}{N} - \gamma\right)I = \gamma\left(\frac{J}{J^*} - 1\right)I.$$

Considering the time derivative of $w(J, I)$, we have

$$\begin{aligned}
\dot{w}(J,I) &= \gamma\left(\frac{\dot{J}}{J^*} - \frac{\dot{J}}{J}\right) + r\left(\frac{\dot{I}}{I^*} - \frac{\dot{I}}{I}\right) \\
&= \gamma\dot{J}\left(\frac{1}{J^*} - \frac{1}{J}\right) + r\dot{I}\left(\frac{1}{I^*} - \frac{1}{I}\right) \\
&= \gamma r J\left(1 - \frac{I}{I^*}\right)\left(\frac{1}{J^*} - \frac{1}{J}\right) \\
&\quad + r\gamma I\left(\frac{J}{J^*} - 1\right)\left(\frac{1}{I^*} - \frac{1}{I}\right) \\
&\text{(substituting for } \dot{I},\ \dot{J}) \\
&= r\gamma\frac{(I^* - I)(J - J^*)}{I^* J^*} \\
&\quad + r\gamma\frac{(I - I^*)(J - J^*)}{I^* J^*} \\
&= 0
\end{aligned}$$

Hence, $w(J, I)$ remains invariant throughout and is equal to $w(J_0, I_0) = w_0$. ■

Proof of Theorem 2(b):
Let $w_0 = w(J_0, I_0)$ be the energy associated with the modified SIR system in Fig 3.2(c). The conservation law implies that every valid state (J, I) corresponds to a point on the level curve given by

$$w(J,I) = \gamma\left(\frac{J}{J^*} - \log\left(\frac{J}{J^*}\right) - 1\right) + r\left(\frac{I}{I^*} - \log\left(\frac{I}{I^*}\right) - 1\right) = w_0.$$

If J, I functions are continuous[5], then these would be periodic functions. In terms of normalized variables, $x = \frac{J}{J^*}$ and $y = \frac{I}{I^*}$, the phase plot reduces to

$$\gamma(x - \log(x) - 1) + r(y - \log(y) - 1) = w_0$$

.

Consider the continuously differentiable function $f(z) = z - \log(z) - 1$ defined on $\mathbb{R}_{++}$. Since $\frac{df}{dz} = 1 - \frac{1}{z}$ and $\frac{d^2 f}{dz^2} = \frac{1}{z^2} > 0$, $f(z)$ is a convex function with a single global minimum at $z = 1$ corresponding to $f(1) = 0$. Hence $f(z) \leq c \Rightarrow z_{min} \leq z \leq z_{max}$ where (z_{min}, z_{max}) correspond to the roots of $f(z) = c$.

To identify the extreme x values, we observe that

$$\begin{aligned}
\gamma(x - \log(x) - 1) + r(y - \log(y) - 1) &= w_0 \\
\Rightarrow \gamma(x - \log(x) - 1) &\leq w_0 \\
(\text{ since } f(y) > 0) & \\
\Rightarrow x_{min} \leq x \leq x_{max} &
\end{aligned}$$

where (x_{min}, x_{max}) are roots of $f(x) = \frac{w_0}{\gamma}$. Both the extreme values of x are realized for $y = 1$. Similarly, the extreme values of y are attained for $x = 1$ and given by (y_{min}, y_{max}) which correspond to the roots of $f(x) = \frac{w_0}{r}$.

■

Proof of Theorem 2(c).
The period of a Lotka-Volterra system has been derived in multiple works [42]. We include the below proof based on Hsu's method [24] for completeness.

[5]Note that J, I are actually discrete population counts and not continuous functions.

Let $x = \frac{J}{J^*}$ and $y = \frac{I}{I^*}$. Then we have

$$\dot{x} = -rx(y-1) \tag{5}$$

$$\dot{y} = \gamma y(x-1). \tag{6}$$

From 5, we have

$$\begin{aligned}
\ddot{x} &= -rx\dot{y} - r\dot{x}(y-1) \\
&= -rx\gamma y(x-1) - r(y-1)\dot{x} && \text{(substituting } \dot{y} \text{ from 6)} \\
&= -r\gamma x(-\frac{\dot{x}}{rx} + 1)(x-1) + \frac{r(\dot{x})^2}{rx} && \text{(substituting y from 5)} \\
&= -\gamma(rx - \dot{x})(x-1) + \frac{\dot{x}^2}{x}
\end{aligned}$$

Thus,

$$\ddot{x} - \frac{\dot{x}^2}{x} - \gamma(x-1)(\dot{x} - rx) = 0. \tag{7}$$

Let $z = \log(x)$. Then, $\dot{x} = e^z \dot{z}$ and $\ddot{x} = e^z(\ddot{z} + \dot{z}^2)$.

From 7, we have

$$\begin{aligned}
e^z(\ddot{z} + \dot{z}^2) - \frac{e^{2z}(\dot{z})^2}{e^z} & \\
-\gamma(e^z - 1)(e^z\dot{z} - re^z) &= 0 \\
\Rightarrow \ddot{z} - \gamma(e^z - 1)(\dot{z} - r) &= 0.
\end{aligned}$$

Choosing $s = \dot{z} \Rightarrow s = \frac{\dot{x}}{x} = -r(y-1)$.

Let $w_0 = w(J_0, I_0)$. Then, the trajectory corresponds to

$$\begin{aligned}
&\gamma(x - \log x - 1) + r(y - \log y - 1) = w_0 \\
&\Rightarrow \gamma(e^z - z - 1) + r(y - \log y - 1) = w_0 \\
&\Rightarrow \gamma(e^z - z - 1) + r(-\frac{s}{r} - \log(1 - \frac{s}{r})) = w_0 \\
&\Rightarrow \gamma(e^z - z - 1) - w_0 = s + r\log(1 - \frac{s}{r}) \\
&\Rightarrow G(z) = F(s)
\end{aligned}$$

where $G(z) = \gamma(e^z - z - 1) - w_0$ and $F(s) = s + r\log(1 - \frac{s}{r})$.

Let $F_1(s), F_2(s)$ be the restrictions of $F(s)$ for the lower and upper parts of the phase plot. Then the time period for the lower section is given by

$$\int_{z_{min}}^{z_{max}} \frac{dz}{s} = \int_{z_{min}}^{z_{max}} \frac{dz}{F_1^{-1}(G(z))}.$$

The total time for both the lower and upper section is given by

$$\int_{\log(x_{min})}^{\log(x_{max})} \left(\frac{1}{F_1^{-1}(G(z))} - \frac{1}{F_2^{-1}(G(z))} \right) dz.$$

When $w_0 \simeq 0$, linearization is possible. Simplifying the trajectory $F(s) = G(z)$ using the approximations $e^a = 1 + a + \frac{a^2}{2}$ and $\log(1-a) = a - \frac{a^2}{2}$, we have

$$\begin{aligned}
&\gamma(e^z - z - 1) - w_0 = s + r\log(1 - \frac{s}{r}) \\
&\Rightarrow \frac{\gamma z^2}{2} - w_0 = s + r(-\frac{s}{r} - \frac{s^2}{2r^2}) \\
&\Rightarrow \frac{\gamma z^2}{2} + \frac{s^2}{2r} = w_0
\end{aligned}$$

Essentially, we have an elliptical curve with x, y following sinusoidal behavior with a period $\frac{2\pi}{\sqrt{r\gamma}}$. ■

Proof of Theorem 2(d).
Assuming a continuous form for J, we observe that

$$\begin{aligned}
\dot{J} &= (r - eI)J \\
\Rightarrow \frac{1}{J}\frac{dJ}{dt} &= r - eI \\
\frac{d}{dt}(\log(J)) &= r - eI \\
\int_{t=t_0}^{t=t_0+T_{period}} d(\log(J)) &= \int_{t=t_0}^{t=t_0+T_{period}} (r - eI)dt \\
&\text{(since } J \text{ is periodic)} \\
\int_{t=t_0}^{t=t_0+T_{period}} d(\log(J)) &= 0 \text{ (for any } t_0) \\
\Rightarrow \int_{t=t_0}^{t=t_0+T_{period}} I dt &= \frac{r}{e}T_{period} \\
&= I^* T_{period}
\end{aligned}$$

In other words, I^* is also the average value of I in each cycle.

Considering the time derivatives of S and I, we have $\dot{I} = \frac{\beta SI}{N} + \gamma I$ and $\dot{S} = -\frac{\beta SI}{N}$.

Let ΔS be the drop in S during a single cycle starting at any t_0, then

$$\begin{aligned}
\Delta S &= \int_{t=t_0}^{t=t_0+T_{period}} \dot{S} dt \\
&= \int_{t=t_0}^{t=t_0+T_{period}} (-\dot{I} + \gamma I)dt \\
&\quad \text{(since } \dot{I} = -\dot{S} + \gamma I) \\
&= 0 + \gamma \int_{t=t_0}^{t=t_0+T_{period}} I dt \\
&\quad \text{(since } I \text{ is periodic)} \\
&= \gamma I^* T_{period} \text{ (from above)}
\end{aligned}$$

■

Proof of Theorem 4.
Assuming a proportional additive control on β of the form $\dot{\beta} = \frac{\beta^2 SI}{N} + (r - eI)\beta + u\beta$, the variation of the susceptible contacts J is given by

$$\begin{aligned}
\dot{J} &= \dot{\beta}S + \beta\dot{S} \\
&= \left(\frac{\beta^2 SI}{N} + (r - eI)\beta + u\beta\right) S \\
&\quad + \beta\left(-\frac{\beta SI}{N}\right) \\
&= (r - eI + u)J
\end{aligned}$$

Let $\mathbf{z} = (J/J^* - 1, I/I^* - 1) = (z_1, z_2)$ so that $\mathbf{z} = (0, 0)$ corresponds to the equilibrium state. Then $w(J, I) = \gamma(z_1 - \log(1 + z_1)) + r(z_2 - \log(1 + z_2))$. For $V(\mathbf{z}) = L(w(J, I), w^*)$ to be a control-Lyapunov function, we require $\dot{V}(\mathbf{z}, \mathbf{u}) < 0$.

$$\begin{aligned}
\dot{V}(\mathbf{z}, \mathbf{u}) &= \langle \nabla V(\mathbf{z}), \dot{\mathbf{z}} \rangle \\
&= \frac{dL}{dw} \langle \nabla w(\mathbf{z}), \dot{\mathbf{z}} \rangle \\
&= \frac{dL}{dw}\left(\frac{dw}{dz_1}\dot{z}_1 + \frac{dw}{dz_2}\dot{z}_2\right) \\
&= \frac{dL}{dw}\left(\gamma\Big(1 - \frac{1}{z_1 + 1}\Big)\dot{z}_1 \right. \\
&\quad \left. + r\Big(1 - \frac{1}{z_2 + 1}\Big)\dot{z}_2\right) \\
&= \frac{dL}{dw}\left(\gamma\Big(\frac{J}{J^*} - 1\Big)u\right).
\end{aligned}$$

When the control is chosen as
$u = -\eta(t)\frac{dL}{dw}(\frac{J}{J^*} - 1)$ and $\eta(t) > 0,\ \forall t$,

$$\begin{aligned}
\dot{V}(\mathbf{z}, \mathbf{u}) &= \frac{dL}{dw}\left(\gamma\Big(\frac{J}{J^*} - 1\Big)\right) \\
&\quad \times \left(-\eta(t)\frac{dL}{dw}\Big(\frac{J}{J^*} - 1\Big)\right) \\
&= -\eta(t)\gamma\left(\frac{dL}{dw}\Big(\frac{J}{J^*} - 1\Big)\right)^2 \\
&< 0 \ \ (\text{unless } w = w^*)
\end{aligned}$$

Hence, Artstein's theorem guarantees convergence to the equilibrium. ■